Accepted Manuscript

Rapid synthesis of C-dot@TiO_2 core-shell composite labeling agent: Probing of complex fingerprints recovery in fresh water

H.J. Amith Yadav, B. Eraiah, R.B. Basavaraj, H. Nagabhushana, G.P. Darshan, S.C. Sharma, B. Daruka Prasad, R. Nithya, S. Shanthi

PII: S0925-8388(17)34447-X

DOI: 10.1016/j.jallcom.2017.12.251

Reference: JALCOM 44337

To appear in: *Journal of Alloys and Compounds*

Received Date: 22 September 2017

Revised Date: 9 December 2017

Accepted Date: 22 December 2017

Please cite this article as: H.J. Amith Yadav, B. Eraiah, R.B. Basavaraj, H. Nagabhushana, G.P. Darshan, S.C. Sharma, B. Daruka Prasad, R. Nithya, S. Shanthi, Rapid synthesis of C-dot@TiO_2 core-shell composite labeling agent: Probing of complex fingerprints recovery in fresh water, *Journal of Alloys and Compounds* (2018), doi: 10.1016/j.jallcom.2017.12.251.

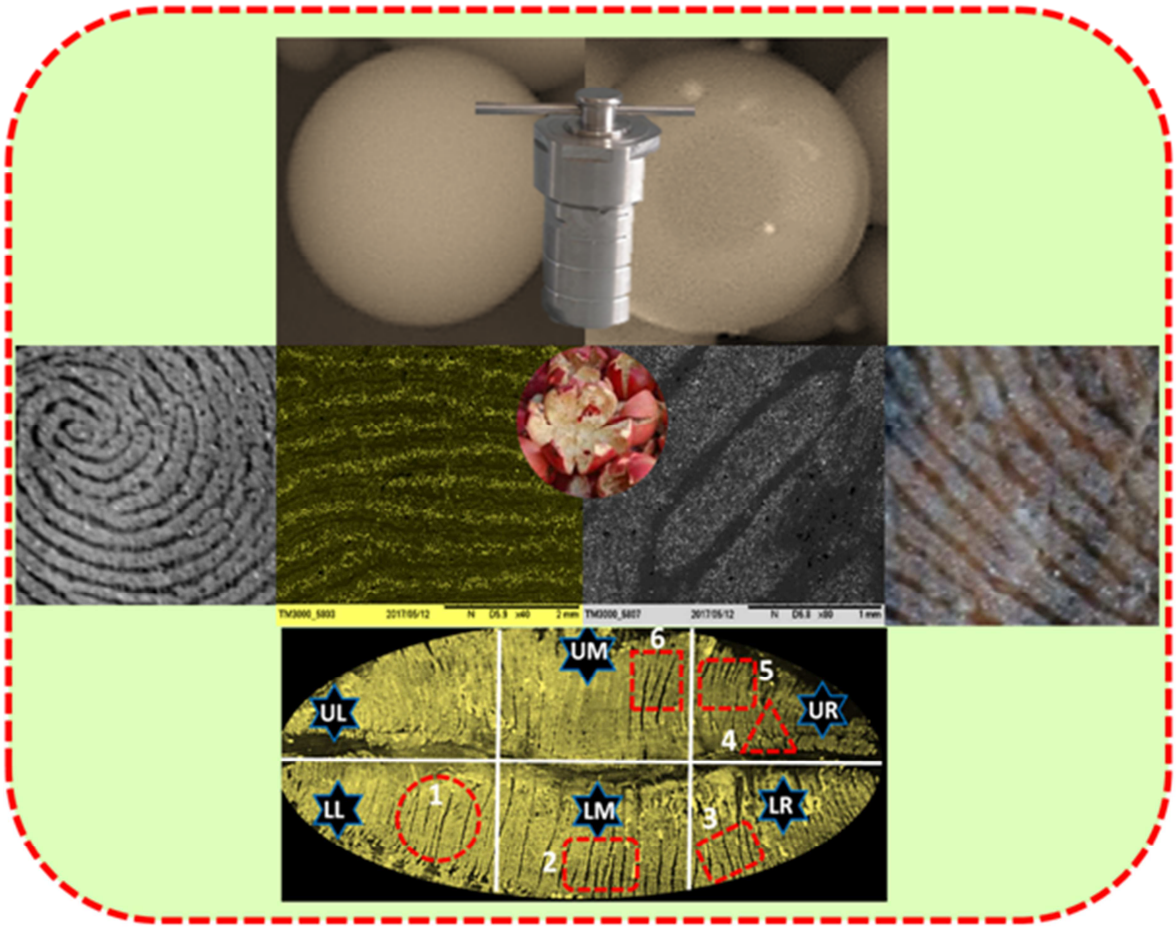

Rapid synthesis of C-dot@TiO_2 core-shell composite labeling agent: Probing of complex fingerprints recovery in fresh water

H.J. Amith Yadav[1], B. Eraiah[1], R.B. Basavaraj[2], H.Nagabhushana[2*], G.P. Darshan[3], S.C. Sharma[4, 5], B. Daruka Prasad[6], R. Nithya[7], S. Shanthi[7]

[1]Department of Physics, Bangalore University, Bangalore -560056, India
[2]Prof.C.N.R. Rao Center for Advanced Materials, Tumkur University, Tumkur-572103, India
[3]Department of Physics, Acharya Institute of Graduate Studies, Bangalore- 560 107, India
[4]Advisor, Avinashilingam Institute for Home Science and Higher Education for Women University, Coimbatore 641043, India
[5]Department of Mechanical Engineering, Jain University, Advisor, Jain group of Institutions, Bangalore 560069, India
[6]Department of Physics, BMS Institute of Technology and Management, VTU-affiliated, Bangalore 560 064, India
[7]Department of Civil Engineering, Avinashilingam Institute for Home Science and Higher Education for Women University, Coimbatore 641043, India

Abstract

A straightforward and facile one-pot synthesis of carbon dots from pomegranate waste peels was performed using the hydrothermal carbonization technique at a gentle temperature (180 °C). The carbon dots/TiO_2 (C-dot@TiO_2) core-shell nanostructures (NSs) are prepared by hydrothermal route. The obtained products are well characterized for their chemical composition and morphological features by different spectroscopic and transmission electron microscopy. The synthesized C-dot@TiO_2 are characterized by transmission electron microscopy (TEM), fluorescence spectrophotometer, UV−Vis absorption spectra as well as Fourier transform infrared spectroscopy (FTIR). The results reveal that the as-prepared C-dots are spherical shape with an average diameter of 6 µm. Powder dusting method is used to visualize latent fingerprints (LFPs) by staining uncoated and carbon coated NSs on various porous and non-porous surfaces under UV light. The optimized powders are also used to recover latent prints submerged in water on different non-porous dried surfaces including aluminum foil, glass, mica sheet and different textured marbles. Also, the duration of submersion affects the quality of FPs developed; the longer the duration, the worse the quality is. It is clear that core-shell NPs display high sensitivity, reproducibility, selectivity, reliability, and can obtain the complete three levels of friction ridge details.

Keywords: Carbon dots; diffuse reflectance spectroscopy; Fingerprint; fresh water; lip print.

* Corresponding author: E-mail: bhushanvlc@gmail.com (H. Nagabhushana).

1. Introduction

Before the trend in nanoparticle research, many detection methods are developed for visualization of LFPs. However, there still exists a scarcity of sensitivity and selectivity. Nanoparticles (NPs) are then proposed as a way to tackle these concerns [1-3]. Their small size, versatility and ability to precisely tune their surface properties are the main objectives why they interest so much consideration. The surface modification versatility of these materials may lead to visualize all the types of FP ridge characters including sweat pores. Their numerous optical properties can lower detection limits and increase the sensitivity, typically by using luminescent properties to get rid of background interference. Till date several types of NPs have been used for fingerprint detection and studied extensively by several methods [4-8].

TiO_2 NPs are considered to be among the best photo catalytic materials due to their long-term thermodynamic stability, strong oxidizing power, and relative non-toxicity. The nanomaterials often show unique and considerably changed physical, chemical and biological properties when compared to their macro scaled counterparts [9-12]. The titanium dioxide and copper have been used mostly for the synthesis of stable dispersions of nanoparticles, which are useful in areas such as photography, catalysis, biological labeling, photonics, optoelectronics and surface-enhanced Raman scattering detection [13]. They have also been recently utilized in many applications such as gas sensing, photochromic devices, and solar cells as well as for their role in drug delivery, diagnostics, imaging, sensing, gene delivery, artificial implants, and tissue engineering [14].

In the recent time, carbon dots (C-dots) have become rising star belonging to the carbonaceous family and have explored substantial attention in numerous research areas because of their benign, abundant and inexpensive nature. C-dots can be a potential candidate emerged as

an alternative for the existing traditional semiconductor quantum dots [15]. They also paid much attention due to their potential applications in bio-imaging, sensor, optoelectronics, photocatalysis, supercapacitors, and so on [16-18].

Till date various techniques have been set up for the preparation of C-dots namely, thermal oxidation, laser ablation, electrochemical oxidation, hot injection, microwave irradiation and pyrolysis [19-21]. These methods have some confinements, for example low item yield, absence of size control and the utilization of poisonous chemicals or high temperature for the preparation. Thus, there is a critical need to set up new techniques, which are cost- effective, environmental friendly and are alternative to the harmful chemical and physical methods.

Hydrothermal carbonization could be a powerful strategy because of its basic exploratory setup, which stays away from the need of emphatically poisonous chemicals or high temperature. Primarily, water is utilized as the response medium for the change of biomass, where the mass as well as nano-sized carbon materials are given under gentle exploratory conditions. In the mean time an economical source of raw materials are used for the preparation of C-dots. In this regard, bio-waste materials can be considered as a viable and potential option feedstock to fossil resources for variety of chemicals [22].

Pomegranate waste peels are one of the most underutilized natural resources and most geographically diverse bio-waste residues on earth, and the huge remnants have never been challenged to utilize extensively in an effective manner. Pomegranate peel extract majorly contains of anthocyanins, polyphenols, ellagic acid, pelargonidin 3-glucoside, cyanidin 3-glucoside, and cyaniding 3, 5-diglucoside [23].

In the present work spherical C-dots are prepared via simple one-step carbonization method, whereby the bio-waste of pomegranate peel extract is processed by the hydrothermal

carbonization at a gentle temperature (180 °C). The dehydration of the pomegranate peel extract leads to the formation of spherical C-dots with an approximate diameter of ~ 6 - 10 µm. Further, TiO_2 layer was coated on the surface of c-dots and the obtained C-dot@TiO_2 NPs were studied in detail for the detection of LFPs on various substrates.

Regardless of the advancements made in DNA profiling, FPs are as yet considered as the most broadly settled types of scientific proof utilized by the forensic scientists to positively recognize a person. Criminal offenders have a key objective not to leave any clues at the crime scene. Some may trust that things recuperated submerged will have no measurable esteem; hence, they endeavor to obliterate these clues by tossing things into the water. Accordingly, it has been the worry of legal specialists to inspect confirmations recuperated from various aquatic conditions. Lawbreakers and law authorization have been stunned by the physical confirmation that remaining parts protected notwithstanding the span of submersion [24, 25].

Regular fingermarks deposits are made of a blend of various substances; 99% water and rest of the part comprises of small traces of organic and inorganic materials. Substrates with non-porous surface usually do not absorb the moisture from the surrounding environment. LFPs on theses non-porous surfaces are more susceptible to harm as the LFP residue accessible on the outermost surface is more exposed to the surrounding environmental factors [26].

Numerous examinations exhibited different components that may impact on the quality of created FPs in water including; individual variation of LFP composition, the nature of surface, time duration after deposition, ecological factors for example, air course, tidy, dampness, light exposure, precipitation, temperature, Ultraviolet rays and synthesis methods [27]. The fingerprint composition varies drastically with respect to the different time durations which in turn may affect the efficiency of the various development techniques. Many authors surveyed

the impact of fresh water on the quality of the developed LFPs using numerous techniques of development, they observed that LFPs are still could be recovered from the substrates which are submerged in the fresh water and they do not have major damage impact.

Lip prints (LPs) convey the extra confirmation to a crime scene that can be important, especially in cases missing other proof, like FPs. LPs can be a factor in several kinds of crimes, such as when a person has been bound or gagged, prints on a glass that a person drank from, prints on a cigarette butt, and prints on a glass/window if they are pressed up against it. All of these are probable places where LPs may be found and used in the examination of a crime [28-30].

Nevertheless, the use of LPs in crime scene is incomplete due to the reliability of LPs has not been decisively recognized in the court of law. Further, LPs are unique and do not alter during the life span of an individual [31]. On the other hand, the major distraction to the lips may lead to scarring, pathosis and the surgical treatment rendered to correct the pathosis may affect the size and shape of the lip, which in turn alter the pattern and morphology of grooves. It has also been proposed that dissimilarities in shapes among males and females could help in sex determination. Lipstick smears can lead to indirect proof of a connection or contact between a victim and a suspect or a suspect and a crime scene. Hence, in addition to the LFPs the LPs are also considerably attracted more interest among the forensic scientists.

Interestingly the precise information of chemical constituents of LFPs is to be known at the time a forensic investigator made attempts to its recovery. Generally, ridge patterns on any surfaces are due to sweat secretions present in the FPs. Major chemical constituents of FPs originating from epidermis, the secretory glands (including three sweat types), intrinsic and extrinsic contaminants such as metabolites, drugs, blood, grease, food contaminants,

moisturizers, hair care products, etc [32]. Even though, these FPs sources certainly contribute to FP residue but they do not give either a comprehensive list or acknowledge probable chemical activity over the time between deposition and visualization. Therefore, many chemical reagents used for visualization of LFPs are developed on this theoretical model of LFP residue there is a motivation to explore further information of the exact chemical composition of LFPs if researchers are to develop new and novel reagents. However, during visualization of LFPs, the substrate on which FPs is deposited is very significant. Generally substrates are broadly classified into two types: porous and non – porous substrates. In the present work, we explored C-dot@TiO_2 NSs to visualize high resolution LFPs on various porous and non-porous surfaces.

Till date no reports are available for the detection of LFPs recovered from the fresh water using C-dot@TiO_2 prepared via hydrothermal carbonization technique. The aim of the present study is to investigate the LFPs developed on various porous and non-porous substrates and their micro-structural analysis. In addition to the LFPs detection the LPs are also investigated under normal light.

2. Experimental

2.1 Hydrothermal Carbonization of pomegranate peel extract

Fig.1. shows the formation of carbon spheres by hydrothermal carbonization process. Pomegranate waste peels are collected from a local fruit shop in Tumkur, India. They are first washed in water and dried in sunlight, followed by oven-drying at 150 °C for 12 h for carbonization. Then, 2 g of the pre-treated Pomegranate waste peels are washed in 60 mL of an aqueous 0.1 M H_2SO_4 solution and rinsed with water, followed by filtering and drying in an oven at 150 °C for 6 h. The obtained Pomegranate peels are then mixed with 60 mL of a sodium hypochlorite (NaClO) solution, kept at room temperature for 6 h and then washed in water with pH of 7. The oxidized Pomegranate peels (in 25 mL of water) are placed in an autoclave by

maintaining the temperature 175 °C for 12 h. Further, it is allowed to cool down to room temperature and the obtained brown precipitate is washed several times with alcohol to remove the un-reacted organic product. The aqueous solution is centrifuged at 7000 rpm for 30 min to separate the solvent from the mixture and finally dried at 120 °C for 3 h.

2.2 Preparation of C-dot@TiO_2 nanostructures

The C-dots@TiO_2 is prepared by hydrothermal method: 25 mg of C-dots and 20 mL of ethanol is dissolved in 40 mL of ultrapure water. The mixtures is ultrasonic dispersion at room temperature for 30 min. Then, 13.2 ml of TBOT is added drop wise into 40 ml of the above solution under vigorous stirring for 2 h. After mixing evenly, they were transferred into a 200 mL stainless steel autoclave with a Teflon liner. The autoclave is treated at 180 ^{o}C for 36 h. After cooling down to room temperature. The white precipitate is filtrated and washed with distilled water for several times. The obtained black brown powders are dried at 100 $^{\circ}$C in a vacuum oven for 10 h and then ground to fine powders with an agate mortar. The synthesis of C-dot@TiO_2 NSs are shown in **Fig.1 (Step.2).**

2.3 Characterization

The prepared samples are characterized by using powder X-ray diffractometer (XRD, Shimadzu 7000) with Cu k_α (1.541 Å) radiation, Hitachi table top (Model TM 3000), Hitachi H-8100 (200 KV), LaB_6 filament equipped with EDS (Kevex sigma TM Quasar, USA). Particle size is estimated by Hitachi (H-8100) made transmission electron microscope (TEM). The Diffuse reflectance (DR) spectroscopy of the samples is recorded on Perkin Elmer (Lambda-35) spectrometer. The Fourier transform infrared (FTIR) studies are done by Perkin Elmer Spectrometer (Spectrum 1000). Raman studies are performed using He-Ne laser (~ 632.8 nm) as the excitation source.

3. Results and discussion

The PXRD patterns of the carbon dots, pure TiO_2 and carbon coated TiO_2 are shown in **Fig.2 (a).** It is noticed from the figure that all the PXRD peaks of TiO_2 exclusively in an anatase (tetragonal) phase (JCPDS 21-1272) after thermal annealing. The average crystallite size is estimated by using Debye – Scherrer's relation [33].

One of the drawback of the diffraction pattern is accurate determination of crystal structure because of the overlapping of the diffraction peaks. Therefore Rietveld refinement analysis is used to create the virtual separation of the overlapped peaks (**Fig.2b**). The Rietveld refinement method is used to estimate the entire powder pattern of the sample with the different refinable parameters and to minimize the difference between the observed and calculated pattern by least squares method. The lattice parameters are evaluated by performing Rietveld refinement using *FULLPROF* suit program [34].

Pseudo-Voigt function has been used in order to fit the several parameters like one scale factor, one zero shifting, six background, three cell parameters, five shape and width of the peaks, one global thermal factor and two asymmetric factors . The refined parameters such as occupancy, atomic functional positions for TiO_2 are studied. The obtained results are in good agreement with the calculated XRD intensity. The refined parameters R_p, R_{wp}, R_{Braggs}, χ^2 values indicates the good fit of the profile.

Spectroscopic measurement of diffuse reflectance in UV-Vis spectral range is used for the determination of the band gap of powder samples. The DR spectra of bare TiO_2 and C-dots@TiO_2 are shown in **Fig.2 (c).** The spectra are recorded in the range of 200 -1100 nm wavelength region at room temperature. It can be seen from the **Fig.2 (c)** that a strong absorption peak for TiO_2 is observed in the range of 350 – 400 nm. A sharp decrease in reflectance started at

about 415 nm for the un-doped TiO_2 samples due to strong absorption. In C-dots@TiO_2, the absorption edge suffered a gradual blue shift. To determine the energy band gap, Kubelka-Munk function is used. The Kubelka–Munk function F (R_∞) and band gap energy ($h\nu$) are estimated by utilizing the following equations [35]:

$$F(R_\infty) = \frac{(1-R_\infty)^2}{2R_\infty} \text{ ---------- (1)}$$

$$h\nu = \frac{1240}{\lambda} \text{ ---------- (2)}$$

where R_∞; reflection coefficient of the sample, λ; the absorption wavelength. The energy band gap values are evaluated and are summarized in **Table.1**. The Kubelka-Munk plots for the $TiO_2$and C-dots@TiO_2 samples used to determine their band gap energy associated with an indirect transition **(Fig.2d).**It can be observed that the indirect band gap increases gradually after carbon coating (C-dots@TiO_2).The energy band gap (Eg) values of TiO_2 and C-dots@TiO_2 is found to be 3.33 & 3.97eV respectively. The increase in the band gap value indicates the blue shift in C-dots@TiO_2 nanostructures.

Raman spectroscopy is a vital technique to study the structural properties of NPs, observing the broadening and shifting of Raman modes associated with particle size. According to the Heisenberg uncertainty principle, the particle size as well as phonon position is given by the relation:

$$\Delta X \, \Delta P \geq h^2/4 \text{ --------- (3)}$$

Where ΔX; particle size, ΔP; phonon momentum distribution, and ħ; reduced Planck's constant. According to the law of conservation of momentum, the particle size reduces, the phonon momentum distribution increases within the particle as a result of broadening as well as shifting

of the Raman bands. **Fig.3a** depicts the Raman spectra of TiO_2 and C-dot@TiO_2 NPs. According to group theory analysis, anatase phase of TiO_2 contain six Raman-active modes (A_{1g} + $2B_{1g}$ + $3E_g$). In the present work the Raman spectrum of an anatase TiO_2 NPs have six allowed modes appeared at 140 (E_g), 194 (E_g), 381 (B_{1g}), 505 (A_{1g}) and 616 cm^{-1} (E_g). Further, the intensity of the Raman modes reduces greatly in carbon doped samples. In order to understand the variations in the spectra more clearly, the position and the full width at half maximum [FWHM] of the 381 (B_{1g}), 505 (A_{1g}) and 616 cm^{-1} (E_g) with the addition of carbon doping. In addition to this the position of the Raman bands shifts towards higher wavenumbers and their intensities decrease drastically. The observation can be attributed to the reduction of particle size. It is well known that as the grain size reduces to the nanometer scale, the vibrational properties of materials are greatly enhanced. Mainly, a volume contraction occurs within the NPs owing to the size-induced radial pressure, which leads to an increase in the force constants because of the decrease in the interatomic distances. In vibrational transitions, the wavenumber varies approximately in proportion to $k_{1/2}$, where k is the force constant. Consequently, the Raman bands shift towards a higher wavenumber due to the increasing force constants. The unexpected reduction in scattering intensity, particularly of the Eg modes (140, 194 and 616 cm^{-1}), may be due to the breakdown of long-range translational crystal symmetry caused by the incorporated defects [36].

FTIR spectra are acquired to determine the ligands on the surface of the CNPs; the results are shown in **Fig. 3b.**Spectra of CNPs displayed many common characteristics. The FTIR peaks at 3411 and 1697 cm^{-1} depicted the stretching vibrations of O-H and C-O; the peaks at 1436 and 1316 cm^{-1} related to the asymmetric and symmetric stretching vibrations of NH and C-N, which did not exist in raw material. The peaks at 2945 and 1183 cm^{-1} owed to the stretching vibrations

of CH_2 and C-C. The presence of carboxylate functional moieties is responsible for creating energy traps which make the CNPs highly fluorescent [37].

Fig.4 shows the SEM images of spherical carbon and differently coated (I-III) C-dot@TiO_2 nanostructures. The solid spherical shaped uniform carbon spheres with an average size of ~ 500 nm. If the uniform surfaced carbon spheres are coated with different layers of TiO_2, core-shell NSs with various morphologies can be obtained with narrow size distribution, high packing densities and low scattering of light is achieved as compared to conventional powder particles having large grains and irregular morphology.

Fig.5 (a-d) shows the TEM images of uncoated carbon dots and C-dot@TiO_2 coated (I-III) NSs respectively. As can be seen from the figure the carbon dots were almost spherical in shape with size 2-5 nm **(Fig.5a).** HRTEM images of carbon dots and C-dot@TiO_2 coated (I-III) NSs were shown in **Fig.5 (e-h)**. Further, the interplanar distance (d) was estimated and found to be ~0.25 nm (carbon dots) and 0.28, 0.31 and 0.33 nm for C-dot@TiO_2 coated (I-III) respectively. In order to confirm the presence of Carbon in the TiO_2, energy-dispersive spectroscopy was used **(Fig.5i)** and the corresponding compositions were represented in Table **(Inset: Fig.5i)**. The spectra clearly revealed that the respective peak corresponds to O, Ti and C composition without any impurity.

The practical suitability of C-dot@TiO_2 (I-III coat) is tested for LFP technology on aluminum foil surface and shown in **Fig.6.** It can be seen that the LFP visualized by C-dot@TiO_2 (III coat) sample exhibits well defined ridge characters on most of the selected surfaces are highly distinct with adequate quality, high fluorescence, and low background interference and a clear pattern to the naked eye, with excellent brightness and contrast under normal light.

Therefore, core – shell C-dot@TiO_2 (III coat) can be explored as an excellent labeling agent for visualization of LFPs via powder brushing method in forensic science.

Fig.7 shows the LFPs visualized by staining optimized C-dot@TiO_2 (III coat) NSs on various non-porous magazine covers under normal light by powder dusting method. Usually, FP residue is usually absorbed into porous surfaces but remains on the surface of non-porous surfaces. The visualized LFPs exhibits clear ridge microstructures with good sensitivity and selectivity due to small particle size and better adherence property of the reagent. This demonstrated the practicability of prepared NP for visualize LFPs on non-porous surfaces.

In order to identify the efficiency of the prepared optimized NPs, an overlapped and individual FPs have been taken and applied on the fingermarks (**Fig.8**). It is clearly showed a minute type I (cores and deltas) and II (ridge endings and bifurcations) ridge patterns in with and without overlapped FPs. Generally FP patterns are categorized in three levels. Level 1 pattern is macro which contain cores as well as deltas, which are not distinct sufficient for recognition. However, in Level 2 particulars refer to minutiae points namely ridge endings and bifurcations, which are clearly distinctive patterns. In level 3 types are well-defined ridges containing sweat pores, ridge path deviations, and edge contours, which are extremely vital quantitative data to identify precise FP detection. **Fig.8** displays three levels of FP ridge patterns in overlapped (complex) and single FPs comprising core (level 1), ridge completion(stage II), divergence (stage II), island/dot (stage II), scar (stage III), and pore (stage III). The magnified images from 1 to 3 level details in the FP established by means of dusting method validated its possibility for fingerprint detection.

Generally FPs patterns are categorized into three different levels. Level 1 pattern exhibits delta, loop and whorl which are not distinct for recognition. However, in Level 2 details refer to

minutiae ridge details namely bifurcation, cross over, lake, hook, short ridge, island and etc. which are clearly distinctive patterns. In level 3 types are well-defined ridges containing sweat pores, ridge path deviations and edge contours, which are considered as extremely vital quantitative data to identify individuals. In the present study the level 2 and level 3 FPs are studied in detail. Close inspection of fingertips reveals that they contain permanent, immutable and unique pores that are distributed on the ridges. The detailed sweat pore identification of individuals is attempted by park et al. [38]. The studies that show that 20–40 pores are most sufficient to create patterns that are required for a human's identity. Regrettably, the visualization of such sweat pores has been considered as most neglected part due rapid, reliable and affordable visualization reagents have not been developed. Although many efforts has been attempted to visualize sweat pores, but they requires expensive and complicated experimental procedures and are unable to distinguishing sweat-secreting active pores. But in the present work, we visualized LFPs by staining optimized C-dot@TiO_2 (III coat) NSs under normal light on textured marbles and aluminum foil surface exhibits level 3 ridge patterns, level 1 and level 2 (bifurcation, eye, delta, enclosure, bridge, ridge ending, and crossover) details is shown in **Fig.9.** Well defined ridge microstructures could be clearly observed without background hindrance or color disruption under normal light, leading to exceptional contrast for visualized FP development. The results evident that the all the FP details from levels I to III are detected and validated their possibility in forensic analysis.

All the LFPs are visualized, assessed and scored according to FP quality assessment scale (Table 1). Score 4 and 5 demonstrates excellent visibility (Type I and II). Score 3 demonstrates poor visibility of ridge features are partly visualized. Score 2 demonstrates bad visibility with no clear friction ridges. Score 1 demonstrates blur with no print is visible.

In order to visualize the effect of water salinity (fresh water) on LFPs developed by the powder dusting method on the various porous and non-porous substrates, it is better to leave the surface 2 h to dry before applying the optimized C-dot@TiO_2 (III coat) NSs. The present study revealed that; successful recovery of good and very good quality of latent FPs is possible following submersion in different aquatic environments. In crime scenes, it's unlikely that fingerprint processing and enhancement takes place immediately after deposition especially in underwater crime scene. Therefore, FPs are examined at different intervals; 1 and 7 days.

Micro structural analysis of LFPs

Fig.10 shows the developed FPs visualized under scanning electron microscope (SEM). It can be observed from the figure that various ridge details of level II and level III are clearly detected under SEM. The FPs with level I ridge details namely, bifurcation, ridge ending, bridge, small ridge, Island, dot, cross-over etc. are clearly detected with high resolution images. The level III FPs consists of sweat pores can also be observed with the help of SEM micrograph.

In the present work, the visualized ridge features of LFPs diminish for longer durations (7 days) of immersion in fresh water (**Fig.11).** However, some of the ridge features of good visibility (score 4) are still detected at 7^{th} day. This result further evident that the practical importance of the powder dusting method and different porous and non-porous substrates. The quality of ridge features developed on various substrates with duration can be explained in the light of the fact that; FP composition changes through various chemical, biological and physical processes. Some of the chemical constituents are lost via several processes namely degradation, metabolism, migration, oxidation, polymerization etc.

The longer aging periods may results in larger degradation of FP components. Generally these changes depends on the changes on lipid components such as fatty acids, wax, esters,

triglycerides, cholesterol and squalene within FPs, as these tend to decrease significantly in concentration over time [39]. In addition, water, bottom mud, sands, length of the submersion and other factors can also affects the LFPs to fade faster. Similarly, several authors confirmed the possibility of recovering FPs deposited on glass slides immersed in river, sea, tap, or distilled water. They found a decrease in LFPs visualization with increasing the duration of immersion. In the present study, the FPs immersed for 1 and 7 days are on average of good to very good visibility (Type I and III).

The present study also demonstrated that, the highest percentage of good and very good quality (score 4, 5) of FPs is detected by powder dusting technique. In contrast, other methods, powder dusting is the best method for development of FPs of various surfaces immersed in stagnant water during different time intervals. LFPs developed on some of the porous and non-porous surfaces are found to have the highest mean visibility score after submersion in fresh water for 1 and 7 days. Mean visibility score of prints developed showed significant decline after 7 days of submersion. Prints submerged in fresh water showed significantly higher mean visibility score using various substrate surfaces including aluminum foil, glass, mica sheet and different textured marbles with various time intervals.

Like FPs, lip prints are also unique, individual characteristics, they are allowed as evidence in criminalistics, and they may be found on surfaces (glass, coffee cup, cigarette butts etc.). Latent lip print established on glass slide using the optimized C-dot@TiO_2 (III coat) NSs under normal light and labeled, as shown in **Fig.12.** As can be seen from figure it is found that lip print patterns not simply comprise of one type alone, but appeared as a mixture of varying types as is also the case in a earlier study showed by Tsuchihashi [40]. The human lips are divided into six different portions namely, upper left, upper middle, upper right, lower left, lower

middle and lower right respectively. The lip prints consist of six different types namely: Type –I consist of horizontal with other grooves, Type-II consist of complete vertical, Type-III consist of incomplete bifurcation, Type-IV consist of X or comma form, Type-V consist of complete branched and Type-VI consist of bifurcation. All the six types of grooves (Type I to VI) are clearly observed due to the smaller and uniform sized NSs.

From the above-mentioned findings, it is noteworthy that the data obtained in this study are quite promising as it indicates the uniqueness and permanence of lip prints. Besides, the procedure of lip print analysis is very simple and inexpensive. Therefore, it may be recommended that the lip prints can be used as a reliable aid to human identification in the field of forensic science.

Conclusions

A novel one-pot synthesis of carbon dots from pomegranate waste peels was performed using the hydrothermal carbonization technique. The results reveal that the as-prepared C-dots are spherical shape with an average diameter of 6 µm. Powder dusting method is used to visualize latent fingerprints (LFPs) by staining uncoated and carbon coated NSs on various porous and non-porous surfaces under UV light. The present study concluded that it is possible to recover latent prints submerged in water on different non-porous dried surfaces including aluminum foil, glass, mica sheet and different textured marbles with the best visualization method using optimized C-dot@TiO_2 (III coat) NSs in fresh water. Also, the duration of submersion affects the quality of FPs developed; the longer the duration, the worse the quality is. This study showed that any piece of evidence recovered from underwater should be tested for prints, no matter the amount of time spent beneath the surface. Further it explores a new possibility in the use of composite fluorescent core shells in visualization of complicated and overlapped LFPs available in crime scenes. The procedure adopted was simple and displays superior performance with more efficiency (because fingerprint development procedure was superficial and fast and could be finished in approximately 30 s for trained investigators), high sensitivity (because of lower

background hindrance and sweat pores can be observed owing to the small particle size) and lesser toxicity.

Acknowledgment

One of the author (SCS) thanks DST-FIST NO.SR/FST/ETT-378/2014 for sanctioning of the project.

References

1. B. Figueroa, Y. Chen, K. Berry, A. Francis, D. Fu, Label-Free Chemical Imaging of Latent Fingerprints with Stimulated Raman Scattering Microscopy, Anal. Chem., 89 (2017) 4468–4473.
2. H. Chen, R. Ma, Y. Chen, L. Fan, Fluorescence Development of Latent Fingerprint with Conjugated Polymer Nanoparticles in Aqueous Colloidal Solution, Appl. Mater. Interfaces, DOI: 10.1021/acsami.6b15951.
3. R.B. Basavaraj, H. Nagabhushana, G.P. Darshan, B. Daruka Prasad, S.C. Sharma, K.N. Venkatachalaiah, Ultrasound assisted rare earth doped Wollastonite nanopowders: Labeling agent for imaging eccrine latent fingerprints and cheiloscopy applications, J. Ind. Eng. Chem. 51 (2017) 90-105.
4. M. Dhanalakshmi, H. Nagabhushana, G.P. Darshan, R.B. Basavaraj, B. Daruka Prasad, Sonochemically assisted hollow/solid $BaTiO_3:Dy^{3+}$ microspheres and their applications in effective detection of latent fingerprints and lip prints, J. Sci.: Adv. Mater. Devices, 2 (2017) 22-23.
5. M. Wang, M. Li, A. Yu, J. Wu, C. Mao, Rare Earth Fluorescent Nanomaterials for Enhanced Development of LFPs, ACS Appl. Mater Interfaces 7 (2015) 28110-28115.
6. R.B. Basavaraj, H. Nagabhushana, G.P. Darshan, B. Daruka Prasad, M. Rahul, S.C. Sharma, R. Sudaramani, K.V. Archana, Red and green emitting CTAB assisted $CdSiO_3$: Tb^{3+}/Eu^{3+} nanopowders as fluorescent labeling agents useful for forensic and display applications, Dyes. Pig., 147 (2017) 364-377.
7. K.N. Venkatachalaiah, H. Nagabhushana, G.P. Darshan, R.B. Basavaraj, B. Daruka Prasad, Novel and highly efficient red luminescent sensor based $SiO_2@Y_2O_3:Eu^{3+}$, M^+ (M^+ = Li, Na, K) composite core–shell fluorescent markers for latent fingerprint recognition, security ink and solid state lightning applications, Sens. Actuators, B., 251 (2017) 310-325.
8. A. Sandhyarani, M.K. Kokila, G.P. Darshan, R.B. Basavaraj, B. Daruka Prasad, S.C. Sharma, T.K.S. Lakshmi, H. Nagabhushana, Versatile core-shell $SiO_2@SrTiO_3:Eu^{3+}$, Li^+ nanopowders as fluorescent label for the visualization of latent fingerprints and anti-counterfeiting applications, Chem. Eng. J., https://doi.org/10.1016/j.cej.2017.06.093.
9. G. Longoni, R.L. Pena Cabrera, S. Polizzi, M. D'Arienzo, C.M. Mari, Y. Cui, R. Ruffo, Shape-Controlled TiO_2 Nanocrystals for Na-Ion Battery Electrodes: The Role of Different Exposed Crystal Facets on the Electrochemical Properties, Nano Lett. 17 (2017) 992–1000.
10. H. Hussain, G. Tocci, T. Woolcot, X. Torrelles, C.L. Pang, D.S. Humphrey, C.M. Yim, D.C. Grinter, G. Cabailh, O. Bikondoa, R. Lindsay, J. Zegenhagen, A. Michaelides, G. Thornton, Structure of a model TiO_2 photocatalytic interface, Nat. Mater. 16 (2017) 461–466.
11. Jaspal Singh, Saif A. Khan, J. Shah, R.K. Kotnala, Satyabrata Mohapatra, Nanostructured TiO_2 thin films prepared by RF magnetron sputtering for photocatalytic applications, Appl. Surf. Sci., 422 (2017) 953-961.
12. A.G. Ilie, M. Scarisoreanu, E. Dutu, F. Dumitrache, A. Banici, C.T. Fleaca, E. Vasile, I. Mihailescu, Study of phase development and thermal stability in as synthesized TiO_2 nanoparticles by laser pyrolysis: ethylene uptake and oxygen enrichment, Appl. Surf. Sci., 427 (2018) 798-806.
13. D. Zhang, C. Ge, J. Wang, T. Zhang, Y. Wu, F. Liang, Single-layer graphene-TiO_2 nanotubes array heterojunction for ultraviolet photodetector application, Appl. Surf. Sci., 387 (2016) 1162-1168.

14. T. Xie, A. Rani, B. Wen, A. Castillo, B. Thomson, R. Debnath, T.E. Murphy, R.D. Gomez, A. Motayed, The effects of surface conditions of TiO_2 thin film on the UV assisted sensing response at room temperature, Thin Solid Films, 620 (2016) 76–81.
15. Y. Yang, X. Ji, M. Jing, H. Hou, Y. Zhu, L. Fang, X. Yang, Q. Chena, C.E. Banks, Carbon dots supported upon N-doped TiO_2 nanorods applied into sodium and lithium ion batteries, J. Mater. Chem. A, 3 (2015) 5648–5655.
16. X. Zhu, X. Yang, C. Lv, S. Guo, J. Li, Z. Zheng, H. Zhu, D. Yang, New Approach to Create TiO_2(B)/Carbon Core/Shell Nanotubes: Ideal Structure for Enhanced Lithium Ion Storage, ACS Appl. Mater. Interfaces, 8 (2016) 18815−18821.
17. H. Xu, X. Yang, G. Li, C. Zhao, X. Liao, Green Synthesis of Fluorescent Carbon Dots for Selective Detection of Tartrazine in Food Samples, J. Agric. Food Chem., 63 (2015) 6707−6714.
18. K.A. Shiral Fernando, S. Sahu, Y. Liu, W.K. Lewis, E.A. Guliants, A. Jafariyan, P. Wang, C.E. Bunker, Y. Sun, Carbon Quantum Dots and Applications in Photocatalytic Energy Conversion, ACS Appl. Mater. Interfaces, 7 (2015) 8363−8376.
19. X.Y Xu, R. Ray, Y.L. Gu, H.J. Ploehn, L. Gearheart, K. Raker, W.A. Scrivens, Electrophoretic analysis and purification of fluorescent single-walled carbon nanotube fragments. J. Am. Chem. Soc., 126 (2004) 12736−12737.
20. Y.P. Sun, B. Zhou, Y. Lin, W. Wang, K.A. Shiral Fernando, P. Pathak, J.M. Mohammed, B.A. Harruff, X. Wang, H.F. Wang, P.J.G. Luo, H. Yang, M.E. Kose, B.L. Chen, L.M. Veca, S.Y. Xie, Quantum-sized carbon dots for bright and colorful photoluminescence. J. Am. Chem. Soc., 128 (2006) 7756−7757.
21. J. Wang, C.F. Wang, S. Chen, Amphiphilic egg-derived carbon dots: rapid plasma fabrication, pyrolysis process, and multicolor printing patterns. Angew. Chem., Int. Ed., 51 (2012) 9297−9301.
22. A. Prasannan, T. Imae, One-Pot Synthesis of Fluorescent Carbon Dots from Orange Waste Peels, Ind. Eng. Chem. Res., 52 (2013) 15673−15678.
23. M.N. Nadagouda, N. Iyanna, J. Lalley, C. Han, D.D. Dionysiou, R.S. Varma, Synthesis of Silver and Gold Nanoparticles Using Antioxidants from Blackberry, Blueberry, Pomegranate, and Turmeric Extracts, ACS Sustainable Chem. Eng., 2 (2014) 1717−1723.
24. S. Madkour, A. sheta, F.B. El Dine, Y. Elwakeel, N. AbdAllah, Development of latent fingerprints on non-porous surfaces recovered from fresh and sea water, Egypt. J. For. Sci. 7:3 (2017) 1-12.
25. M. Trapecar, Fingerprint recovery from wet transparent foil. Egypt. J. For. Sci. 2 (2012) 126–130.
26. M. Trapecar, Finger marks on glass and metal surfaces recovered from stagnant water. Egypt. J. For. Sci. 2 (2012) 48–53.
27. R. Rohatgi, A.K. Kapoor Development of latent fingerprints on wet nonporous surfaces with SPR based on basic fuchsin dye. Egypt. J. For. Sci. 6 (2016) 179–184.
28. M. Dhanalakshmi, H. Nagabhushana, G.P. Darshan, R.B. Basavaraj, B. Daruka Prasad, Sonochemically assisted hollow/solid $BaTiO_3$:Dy^{3+} microspheres and their applications in effective detection of latent fingerprints and lip prints, J. Sci.: Adv. Mater. Devices, 2 (2017) 22-23.
29. Vishal Sharma, Amrita Das, Vijay Kumar, Vinay Kumar, Kartikey Verma, H.C. Swart, Combustion synthesis and characterization of blue long lasting phosphor $CaAl_2O_4$: Eu^{2+},

Dy^{3+} and its novel application in latent fingerprint and Lip mark detection, Physica B: Phy. Cond. Matt. http://dx.doi.org/10.1016/j.physb.2017.07.019.
30. M.A. Eldomiaty, R.I. Anwar, S.A. Algaidi, Stability of lip-print patterns: A longitudinal study of Saudi females, J. Forensic. Legal Med., 22 (2014) 154-158.
31. N. Kapoor, A. Badiye, A study of distribution, sex differences and stability of lip print patterns in an Indian population, Saudi J. Bio. Sci., https://doi.org/10.1016/j.sjbs.2015.01.014.
32. M. Pyo, J. Lee, W. Baek, C.W. Lee, B.J. Park, J. Kim, Sweat pore mapping using a fluorescein–polymer composite film for fingerprint analysis, Chem. Comm. 51 (2015) 3177—3180.
33. S.K. Warkhade, G.S. Gaikwad, S.P. Zodape, U. Pratap, A.V. Maldhure, A.V.Wankhade, Low temperature synthesis of pure anatase carbon doped titanium dioxide: An efficient visible light active photocatalyst, Mater. Sci. Semicond. Process. 63 (2017) 18-24.
34. A.K. Tripathi, M.C.B Mathpal, P. Kumar, M.K. Singh, S.K. Mishra, R.K. Srivastava, J.S. Chung, G. Verma, M.M. Ahmad, A. Agarwal, Synthesis based structural and optical behavior of anatase TiO_2 nanoparticles, Mater. Sci. Semicond. Process. 23 (2014) 136-143.
35. R.B. Basavaraj, H. Nagabhushana, B. Daruka Prasad, S.C. Sharma, K.N. Venkatachalaiah, Mimosa pudica mediated praseodymium substituted calcium silicate nanostructures for white LED application, J. Alloys Compd., 690 (2017) 730-740.
36. S. Husain, L.A. Alkhtaby, E. Giorgetti, A. Zoppi, M.M. Miranda, Influence of cobalt doping on the structural, optical and luminescence properties of sol-gel derived TiO_2 nanoparticles, Philos. Mag., 97 (2017) 17–27.
37. H. Yu, Y. Zhao, C. Zhou, L. Shang, Y. Peng, Y. Cao, L. Wu, C. Tung, T. Zhang, Carbon quantum dots/TiO_2 composites for efficient photocatalytic hydrogen evolution, J. Mater. Chem. A, 2 (2014) 3344–3351.
38. D. Park, B.J. Park, J. Kim, Hydrochromic Approaches to Mapping Human Sweat Pores, Acc. Chem. Res., 49 (2016) 1211–1222.
39. S. Pleik, B. Spengler, T. Schafer, D. Urbach, S. Luhn, D. Kirsch, Fatty Acid Structure and Degradation Analysis in Fingerprint Residues, J. Am. Soc. Mass Spectrom. 27 (2016) 1565-1574.
40. Y. Tsuchihashi, Studies on personal identification by means of lip prints, Forensic. Sci. 3 (1974) 233-248.

Figure Captions:

Fig.1 Schematic illustration for the formation of C-dots from the hydrothermal treatment of pomegranate waste peels and C-dot@TiO_2 nanostructures.

Fig.2 (a) PXRD patterns of carbon dots, TiO_2 and C-dot@TiO_2, (b) Rietveld refinement (Inset: Packing diagram) TiO_2, (c) diffuse reflectance spectra and (d) energy band gap plots of TiO_2 and C-dot@TiO_2 nanostructures.

Fig.3 (a) Raman spectra and (b) FTIR spectra of TiO_2 and C-dot@TiO2 NSs.

Fig.4 SEM micrographs of carbon spheres and C-dot@TiO2 (coat I-III) NSs.

Fig.5 (a - d) TEM images, (e – h) magnified TEM, (i – l) HRTEM image, (m – p) SAED patterns of carbon dots, C-dot@TiO_2 (coat – I), C-dot@TiO_2 (coat – II) and C-dot@TiO_2 (coat – III) NSs respectively. (q) EDS spectra of C-dot@TiO_2 (coat – III) NSs.

Fig.6 Fingerprint development on aluminum foil surface using, carbon dots, TiO_2, C-dot@TiO2 (coat-I), C-dot@TiO_2 (coat-II) and C-dot@TiO_2 (coat-III) respectively.

Fig.7 FPs developed on different non-porous magazine covers by optimized C-dot@TiO_2 (III coat) NSs.

Fig.8 Complex and single FPs developed on glass surface using optimized C-dot@TiO_2 (III coat) NSs showing 1 to 3 levels of fingerprint ridge details.

Fig.9 FPs developed on different textured marbles and aluminum foil surface by optimized C-dot@TiO_2 (III coat) NSs showing various ridge details.

Fig.10 Fingerprint ridge details visualized under scanning electron microscope.

Fig.11 Developed FPs using optimized C-dot@TiO_2 (III coat) NSs on various substrate surfaces: aluminum foil, glass, mica sheet and textured marbles before and after submersion in fresh water for 7 days.

Fig.12 Lip print developed using the optimized C-dot@TiO_2 (III coat) NSs under normal light, and their identification traits are labeled.

Table Captions:

Table.1 Fingerprint development scores using optimized C-dot@TiO_2 (III coat) NSs prepared via powder dusting method on aluminum foil, glass, mica sheet and different textured marble surfaces submerged in fresh water at 1, 2 and 7 days intervals according to FPs quality assessment scale.

Table.1 Fingerprint development scores using optimized C-dot@TiO_2(III coat) NSs prepared via powder dusting method on aluminum foil, glass, mica sheet and different textured marble surfaces submerged in fresh water at 1 and 7 days intervals according to FPs quality assessment scale.

C-dot@TiO_2	Time (days)	No. of deposited marks	Scores									
			5 (very good)		4 (good)		3 (poor)		2 (bad)		1 (blur/no)	
			N	%	N	%	N	%	N	%	N	%
Aluminum foil	1	10	10	100	0	0	0	0	0	0	0	0
	7	10	8	80	2	20	0	0	0	0	0	0
Glass	1	10	10	100	0	0	0	0	0	0	0	0
	7	10	7	70	0	0	2	20	1	10	0	0
Mica sheet	1	10	10	100	0	0	0	0	0	0	0	0
	7	10	6	60	3	30	1	10	0	0	0	0
Marbles	1	10	10	100	0	0	0	0	0	0	0	0
	7	10	9	90	1	10	0	0	0	0	0	0

Fig.1. Schematic illustration for the formation of C-dots from the hydrothermal treatment of pomegranate waste peels and C-dot@TiO_2 nanostructures.

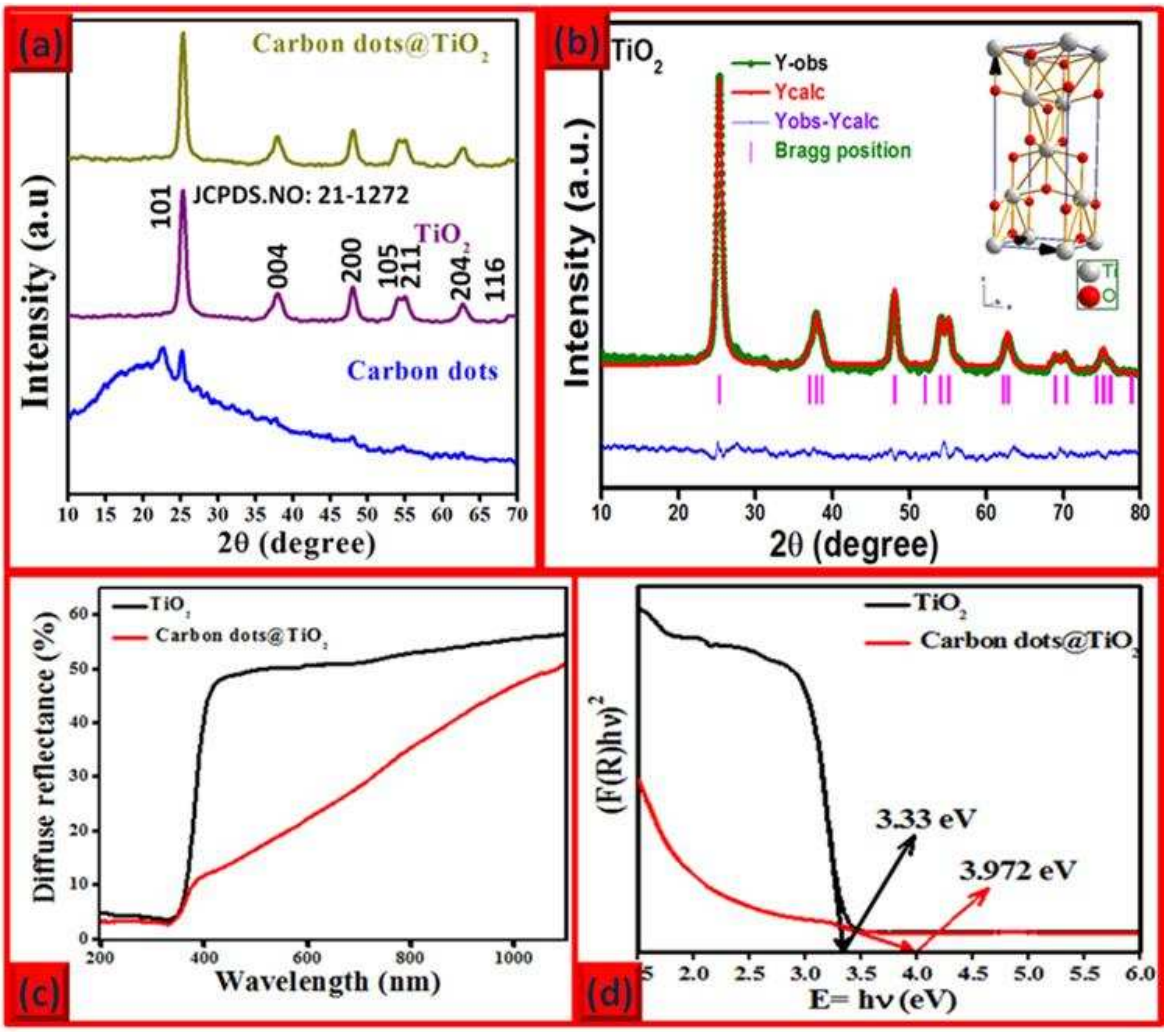

Fig.2(a) PXRD patterns of carbon dots, TiO_2 and $C@TiO_2$, (b) Rietveld refinement (Inset: Packing diagram) TiO_2, (c) diffuse reflectance spectra and (d) energy band gap plots of $TiO_2$and $C@TiO_2$ nanostructures.

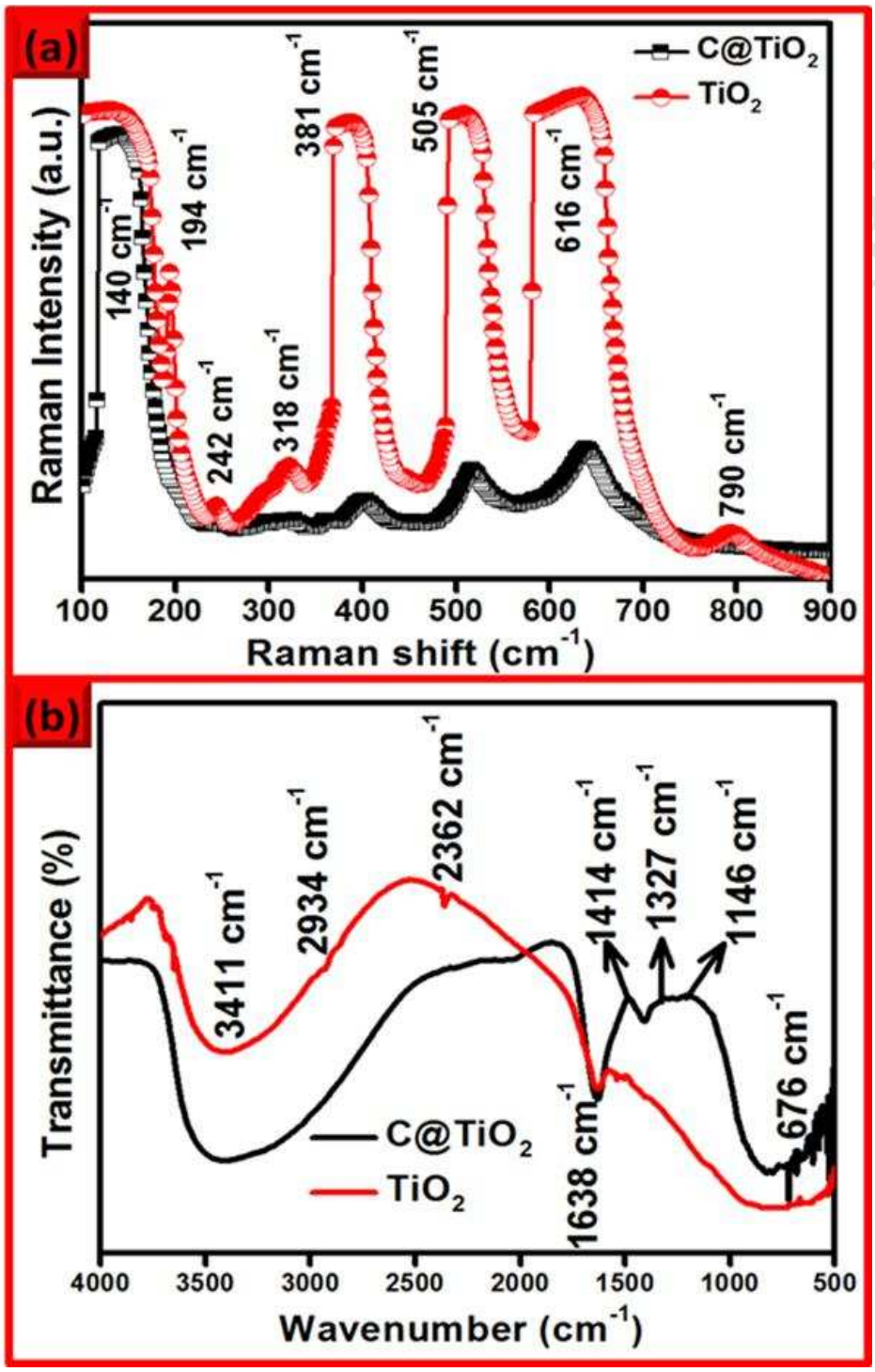

Fig.3 (a) Raman spectra and (b) FTIR spectra of TiO_2 and $C@TiO_2$ NSs.

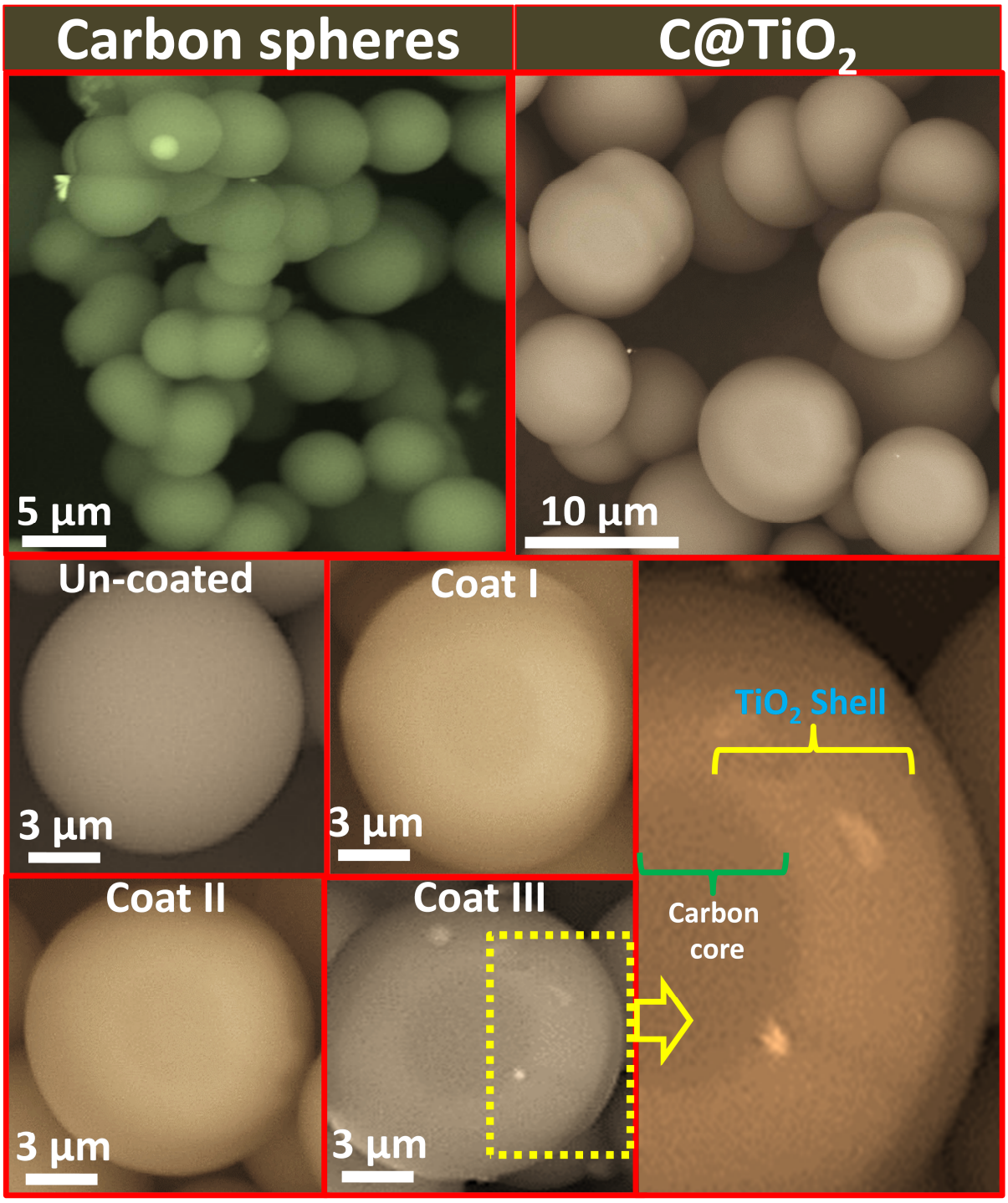

Fig.4 SEM micrographs of carbon spheres and C@TiO_2 (coat I-III) NSs.

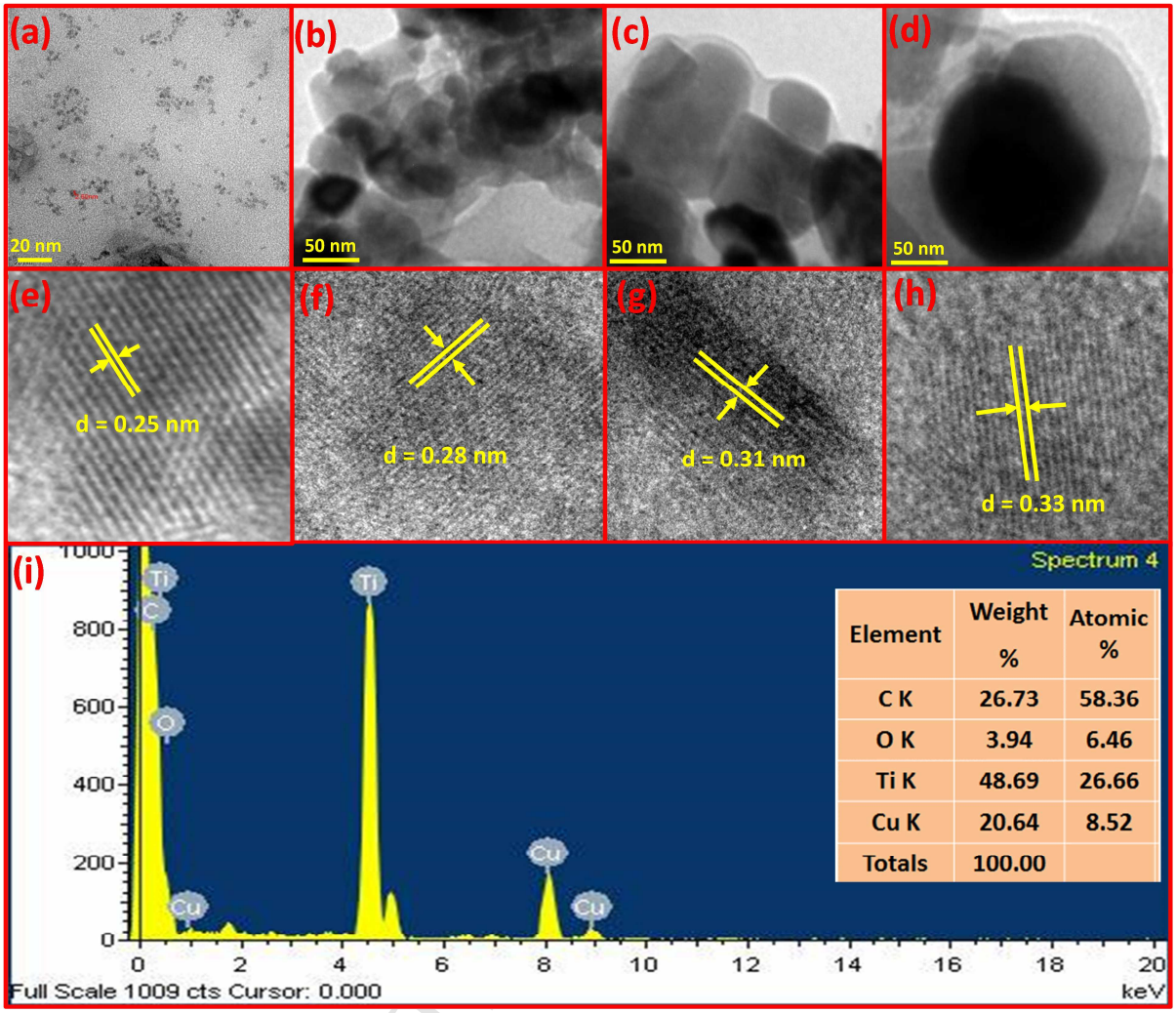

Fig.5 (a - d) TEM images, (e – h) HRTEM image of carbon dots, C-dot@TiO_2 (coat – I), C-dot@TiO_2 (coat – II) and C-dot@TiO_2 (coat – III) NSs (i) EDS spectrum of C-dot@TiO_2 (coat – III) NSs.

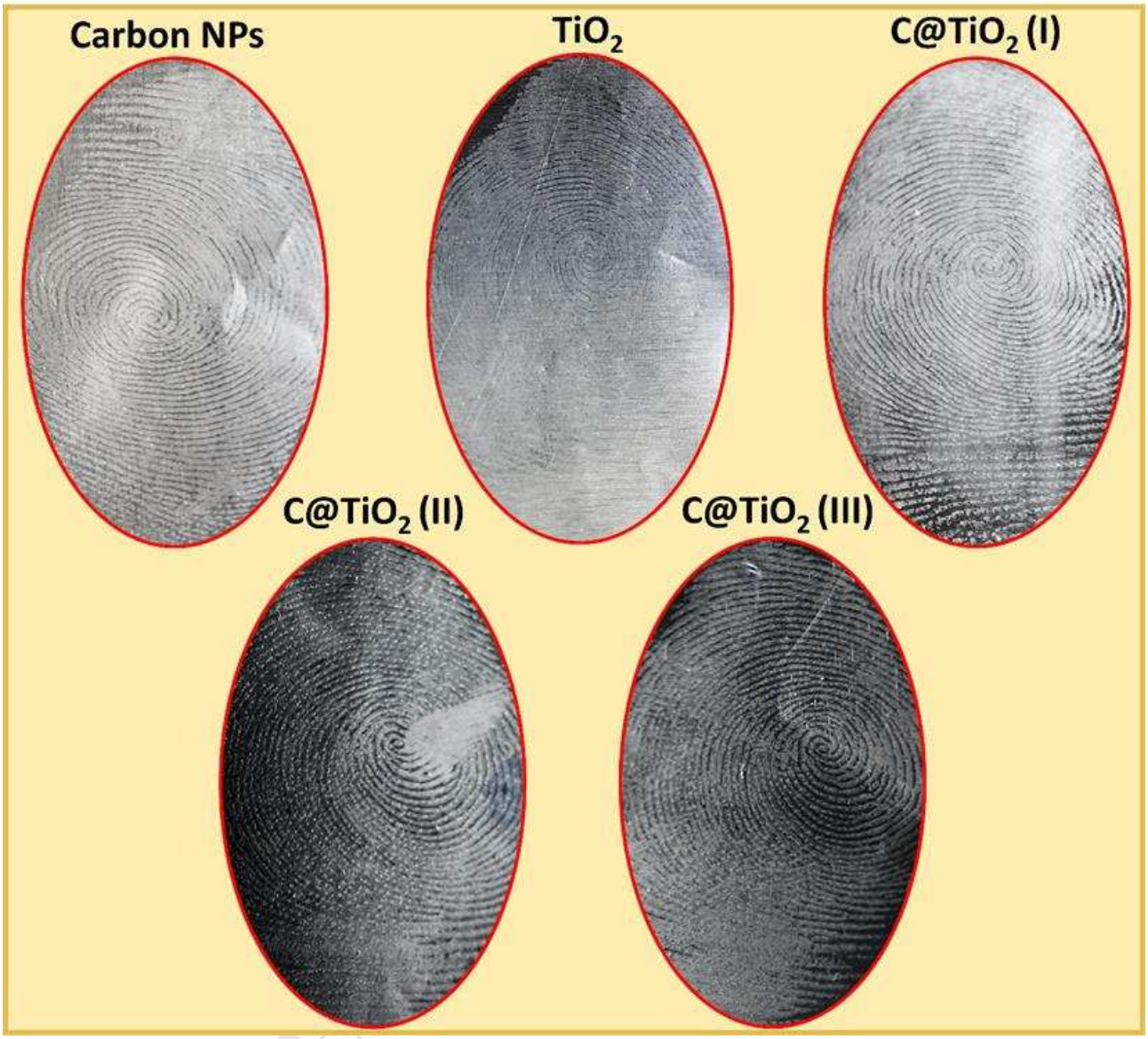

Fig.6 Fingerprint development on aluminum foil surface using, carbon dots, TiO_2, $C@TiO_2$ (coat-I), $C@TiO_2$ (coat-II) and $C@TiO_2$ (coat-III) respectively.

Fig.7 FPs developed on different non-porous magazine covers by optimized C-dot@TiO_2 (III coat) NSs.

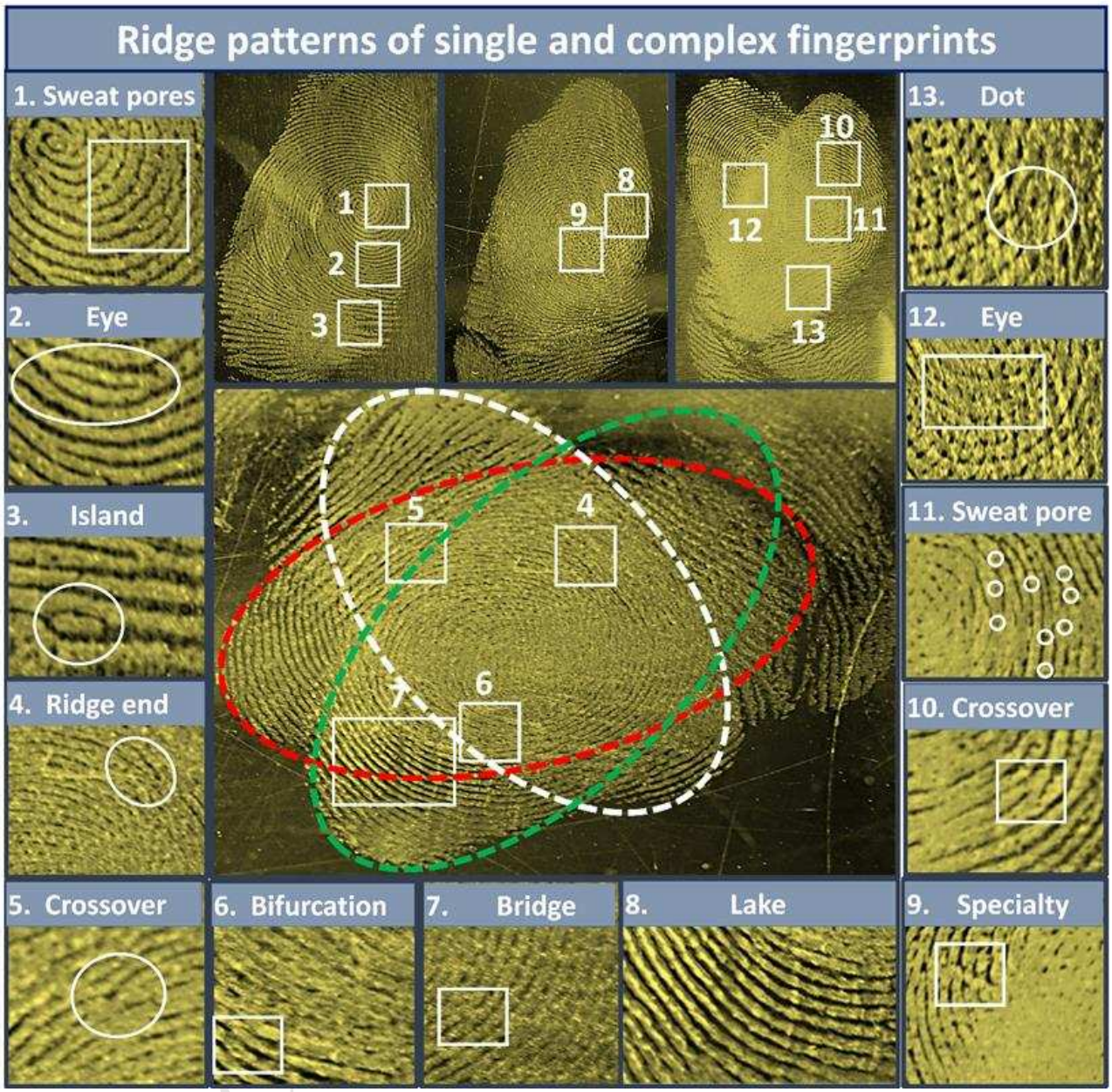

Fig.8 Complex and single FPs developed on glass surface using optimized C-dot@TiO_2 (III coat) NSs showing 1 to 3 levels of fingerprint ridge details.

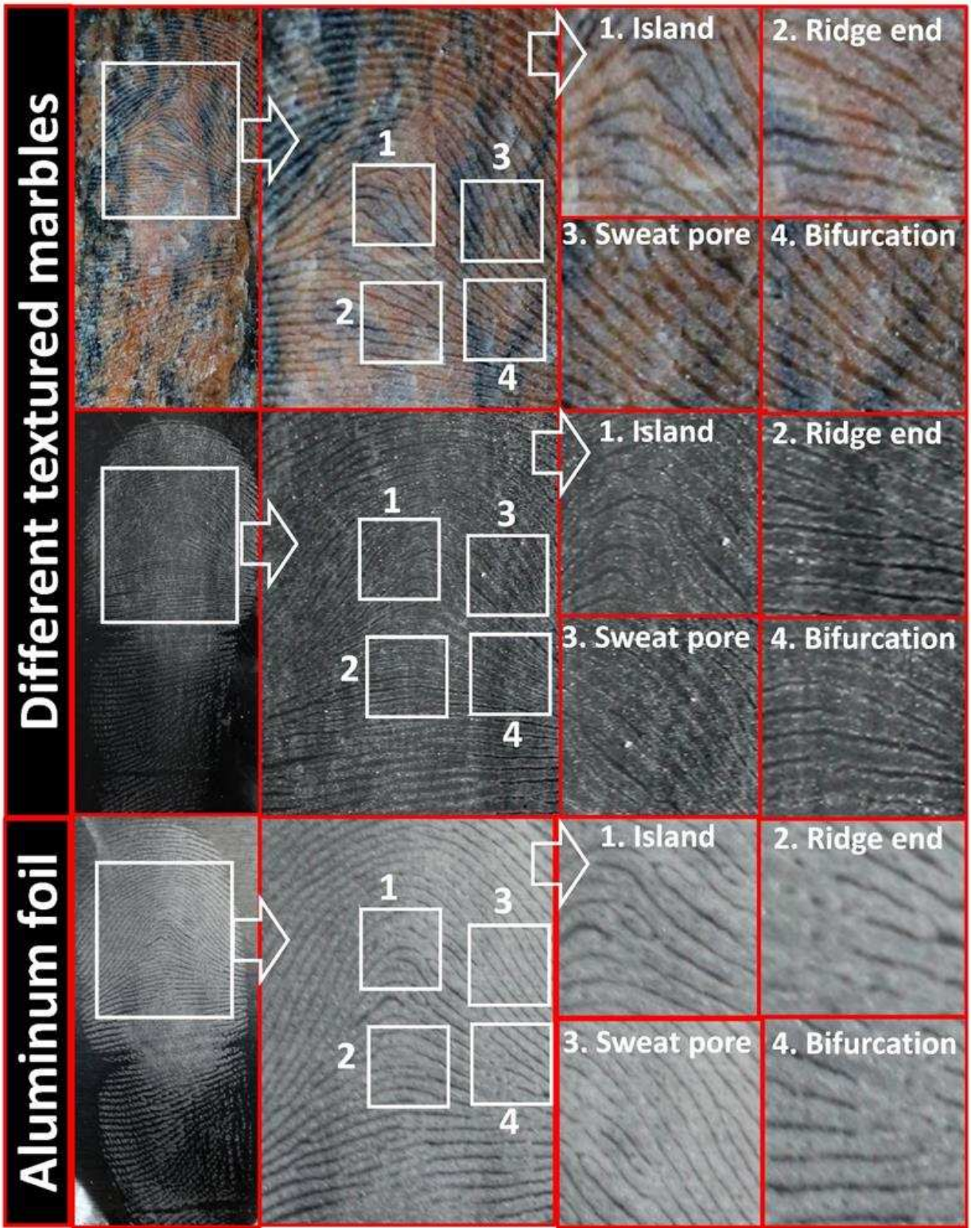

Fig.9 FPs developed on different textured marbles and aluminum foil surface by optimized C-dot@TiO_2 (III coat) NSs showing various ridge details.

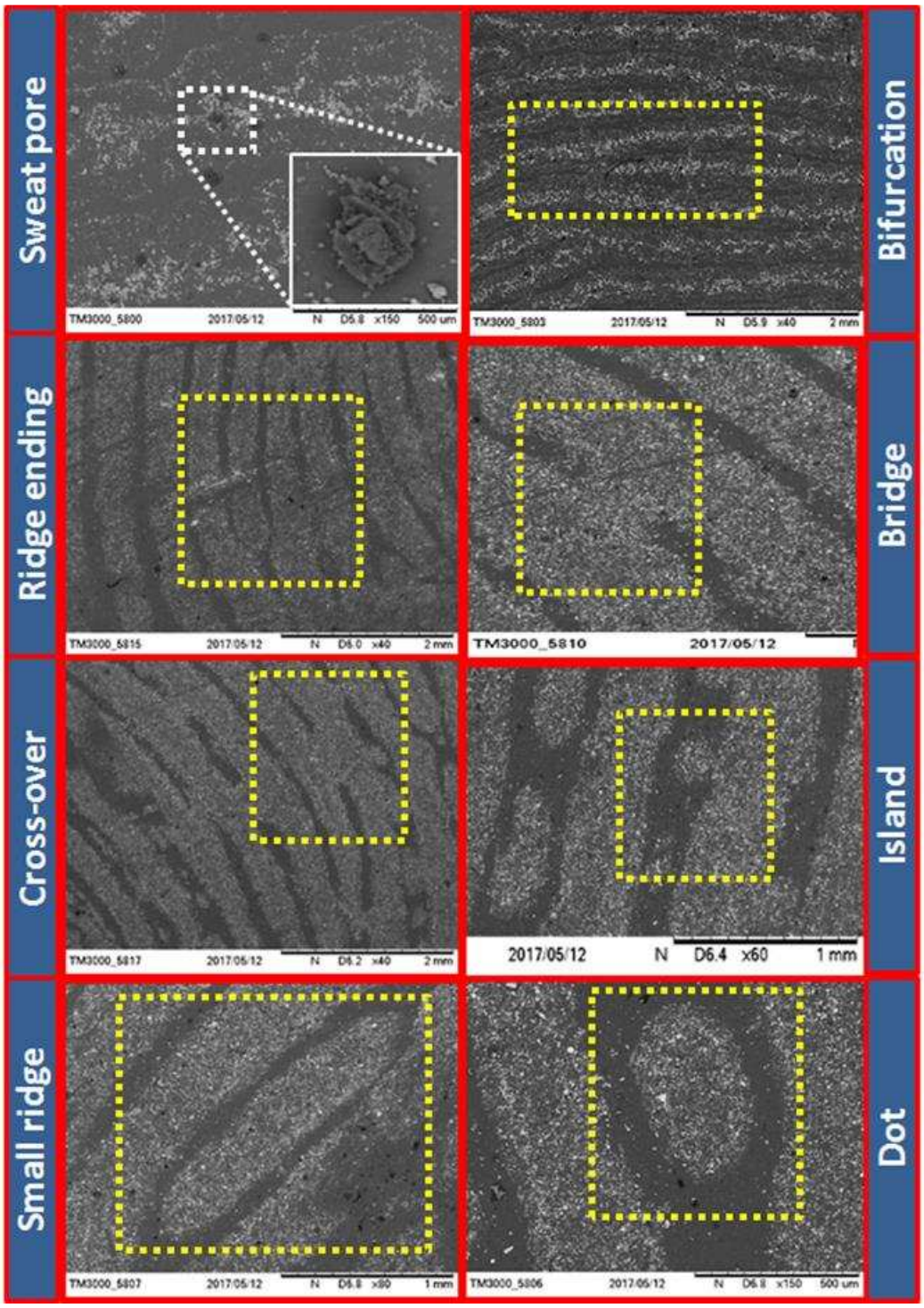

Fig.10 Fingerprint ridge details visualized under scanning electron microscope.

Fig.11 Developed FPs using optimized C-dot@TiO_2 (III coat) NSs on various substrate surfaces: aluminum foil, glass, mica sheet and textured marbles before and after submersion in fresh water for one and seven days.

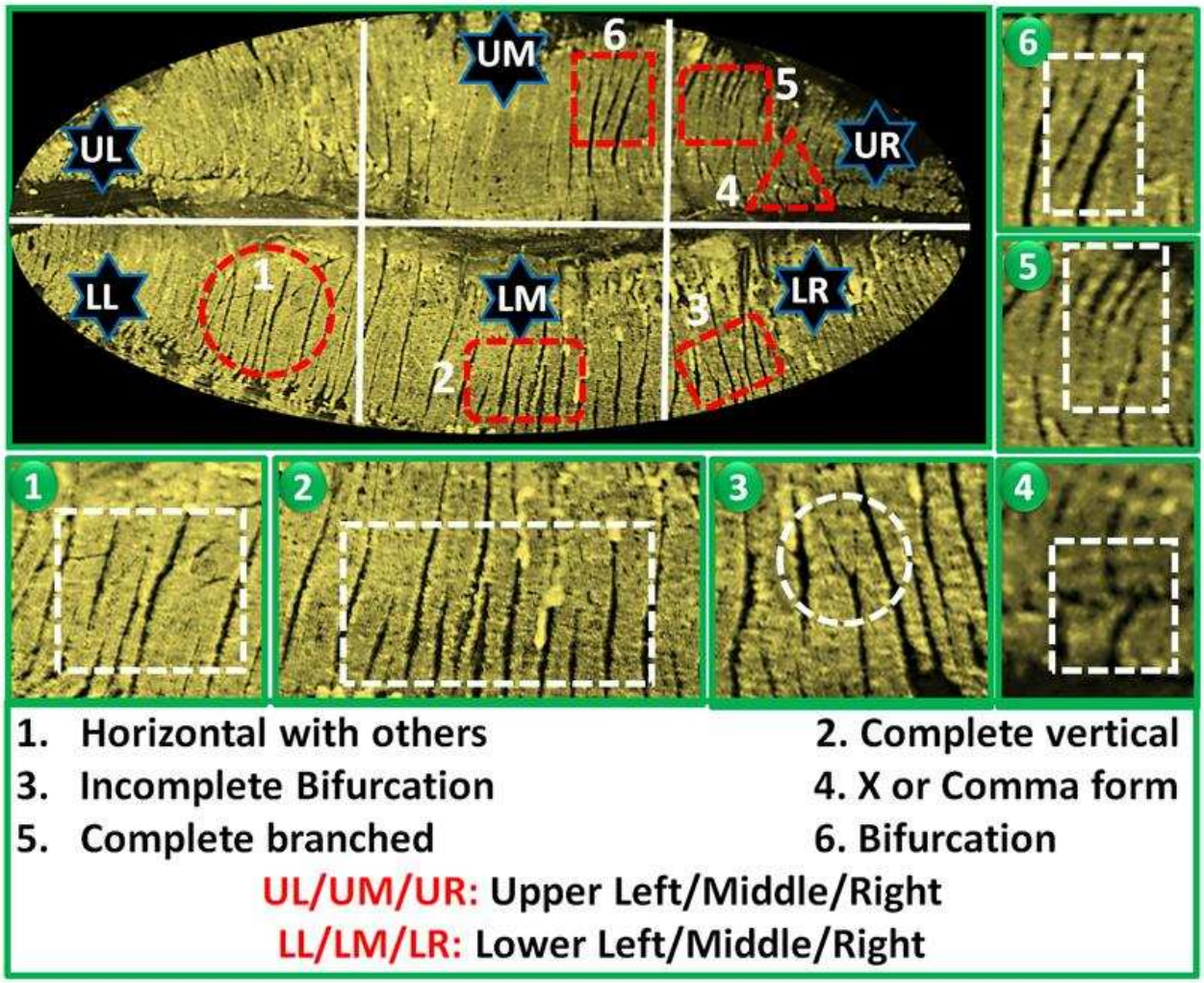

Fig.12 Lip print developed using the optimized C-dot@TiO_2 (III coat) NSs under normal light, and their identification traits are labeled.

Research highlights

1. C-dots are preapred via hydrothermal carbonization of pomogranate peel extract.
2. LFPs are visualized using C-dot@TiO_2 core-shell composites on various porous and non-porous surfaces.
3. Powder dusting method is used to visualize the LFPs submerged in water.